

## RESEARCH ARTICLE



# Admittance spectroscopy analysis of dye-sensitised solar cells with host-guest complexes

**OPEN ACCESS**

Received: 09-04-2020

Accepted: 04-05-2020

Published: 10-06-2020

Editor: Dr. Natarajan Gajendran

**Citation:** Al-Dmour H (2020) Admittance spectroscopy analysis of dye-sensitised solar cells with host-guest complexes. Indian Journal of Science and Technology 13(16): 1686-1692. <https://doi.org/10.17485/IJST/v13i16.215>

**\*Corresponding author.**

Hmoud Al-Dmour

Department of Physics, Faculty of Science, Mu'tah University, Mu'tah, 61710, Jordan.

Tel.: 00962795586638

[hmoud79@mutah.edu.jo](mailto:hmoud79@mutah.edu.jo)**Funding:** None**Competing Interests:** None

**Copyright:** © 2020 Al-Dmour. This is an open access article distributed under the terms of the [Creative Commons Attribution License](https://creativecommons.org/licenses/by/4.0/), which permits unrestricted use, distribution, and reproduction in any medium, provided the original author and source are credited.

Published By Indian Society for Education and Environment ([iSee](https://www.isee.org/))

Hmoud Al-Dmour<sup>1\*</sup>

<sup>1</sup> Department of Physics, Faculty of Science, Mu'tah University, Mu'tah, 61710, Jordan.  
Tel.: 00962795586638

## Abstract

**Objective:** The objective of this study was to assess the influence of encapsulation of cis-bis(isothiocyanato)(2,2'-bipyridyl-4,4'-dicarboxylato)(4,4'-di-nonyl-2'-bipyridyl) ruthenium(II) (Z907 dye) to macrocycle cucurbit[7]uril (CB7) (host) on the performance of nanocrystalline titanium dioxide (nc-TiO<sub>2</sub>)/ poly3-hexylthiophene (P3HT) heterojunction solar cell. **Method:** Two solar cells composed of five layers with and without the encapsulation of Z907 dye on the top of TiO<sub>2</sub> film were used. The admittance spectroscopy was measured at different frequencies to confirm the modification of the interfacial layers' properties in solar cells. **Findings:** The results demonstrated different capacitance responses depending on the voltage applied to the devices. The encapsulated device had a higher capacitance response to forward bias and reverse bias than the non-encapsulated device at the same frequency. The negative capacitance of the two devices was also observed. The results were attributed to an increase in the accumulation of charge carriers and the formation of electric dipoles at the junction which rapidly decreased the capacitance to negative values. **Application:** This study demonstrated that using encapsulation of dye improved the solar cells' maximum electric power to 0.14mW/cm<sup>2</sup>, while it was 0.04 mW/cm<sup>2</sup> in the non-encapsulated solar cells.

**Keywords:** Solar cells; Junction capacitance; X-ray diffraction; SEM micrograph; Geometric capacitance

## 1 Introduction

The efficiency of dye-sensitised solar cells (DSSCs) depends on parameter such as the band gap, molecular structure, morphology, and thickness of the components (hole transport layer, dyes, and oxide materials)<sup>(1-4)</sup>. Oxide materials (such as CeO<sub>2</sub>, nc-TiO<sub>2</sub>, ZnO, and SnO<sub>2</sub>) are electron acceptors used as layers that are deposited directly onto TCO or mixed with a hole conductor to form a larger surface area and greater interfacial electron separation<sup>(5,6)</sup>. However, DSSCs can be challenging to fabricate, The formation of closely packed dye aggregates via intermolecular interactions on the surface can minimise the interfacial charge recombination dynamics at the junction between the polymer and dye layer<sup>(7,8)</sup>. To overcome these challenges, many studies have been conducted to avoid dye aggregation in DSSCs. Seigoito<sup>(9)</sup> reported that ruthenium

complexes (black dye and N719) demonstrate the best results using chenodeoxycholic acid (CDCA), which functions as an anti-aggregation reagent and improves the photovoltaic effect. Water in the dye solution significantly decreases surface dye aggregation, improving solar cell performance of N719<sup>(10)</sup>. In the previous studies<sup>(3)</sup>, the best solar cell performance was achieved in films with the highest RMS roughness and a columnar morphology, the highest external quantum efficiencies (EQEs), and open circuit voltage compared with smoother nc-TiO<sub>2</sub> films. In addition, the encapsulation of the guest (dye) molecule inside the host's organic molecules (supramolecular) prevents dye aggregation and obtains more optimal DSSC performance<sup>(11)</sup>. We demonstrated that the encapsulation of Z907 dye (guest) inside macrocycle cucurbit[7]uril (CB7) (host) can modify the interfacial properties of DSSCs. It decreases the dye aggregation effect between P3HT infused into mesoporous nanocrystalline titanium dioxide (nc-TiO<sub>2</sub>). Devices with and without host-guest complexes have been studied using admittance spectroscopy analysis. Comparing the AC and DC characteristics of the devices confirmed that the encapsulation of dye may improve the performance of DSSCs

## 2 Device fabrication

Figure 1 shows the molecular structures of the materials used to fabricate the devices. The devices were composed of five layers. The bottom electrode was fluorine-doped tin oxide (SnO<sub>2</sub>:F) coated with a thin, compact layer of titanium dioxide TiO<sub>2</sub> deposited using spray pyrolysis. nc-TiO<sub>2</sub> (Ti-nanoxide T) sol-gel was spread over the compact TiO<sub>2</sub> layer using doctor blade technique and treated at 450 °C for 30min<sup>(12)</sup>. The nc-TiO<sub>2</sub> film's colour changed from whitish to yellowish and then became transparent. The film was soaked in CB7 solution with a concentration of 0.8 mM in pure H<sub>2</sub>O for 12 h<sup>(13)</sup>. Before sensitising the resulting layer, the CB7/nc-TiO<sub>2</sub> film was dried under a nitrogen flow for 3 min. The CB7/nc-TiO<sub>2</sub> film was then soaked in a solution of 10 mg ruthenium 535 and 50mL of pure ethanol. The film was then rinsed in ethanol and dried under a nitrogen stream. A 1ml drop of p-type organic semiconductor P3HT in chloroform (15 mgmL<sup>-1</sup>) was placed onto the surface of the sensitized layer and left for several seconds prior to spinning at 1000 rpm. The device was completed by evaporating gold electrodes with an area of 3mm<sup>2</sup> onto the P3HT. A Keithley model 307 source measurement unit and an Agilent E4980A precision LCR meter were used to study the current vs the voltage and the capacitance vs the voltage under different conditions respectively. A xenon lamp was used to illuminate the devices. The X-ray diffraction (XRD) patterns were obtained using a Seifert 3003 TT diffract meter operating at 40 kV and 40 mA. The nc-TiO<sub>2</sub> thin film's microstructure was assessed by a Cambridge Stereoscan-360 scanning electron microscope operating at 20 kV.

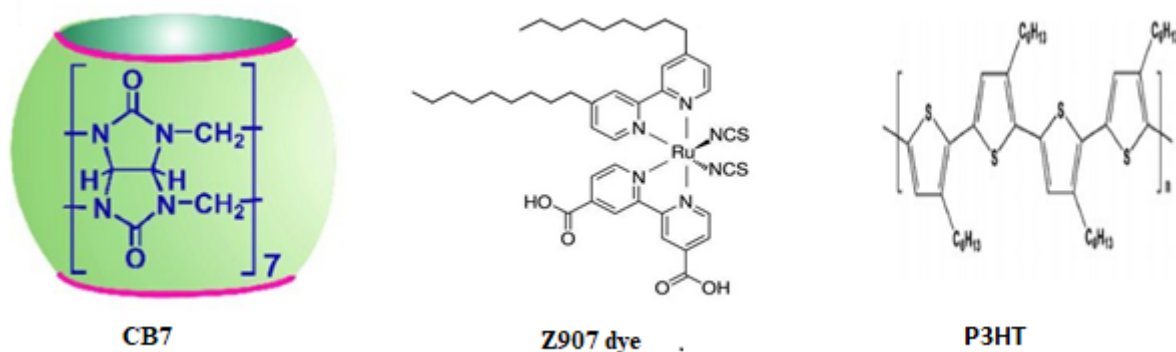


Fig 1. Chemical structure of macrocyclecucurbit[7]uril (CB7), ruthenium (Z907dye), and poly(3-hexylthiophene)(P3HT)

## 3 Results

Figure 2 shows the X-ray diffraction spectroscopy (XRD) patterns of the mesoporous non-crystalline titanium dioxide (nc-TiO<sub>2</sub>) coated on a glass substrate with  $2\theta = 20-80$ . The sample's XRD patterns exhibited diffraction angles (peak positions) corresponding to the anatase phase of TiO<sub>2</sub>. This agreed with JCPDS card no. 21-1272 (anatase TiO<sub>2</sub>) and the XRD patterns of TiO<sub>2</sub> nanoparticles reported in the literature<sup>(14)</sup>. The peak positions occurred at 25°, 48° and 54°. The three peaks were indexed to the (101), (200), and (105) lattice planes of the nc-TiO<sub>2</sub>, respectively. The grain sizes of the nc-TiO<sub>2</sub> film were computed by

applying Scherrer's formula to the high-intensity peak<sup>(15)</sup>. The crystal size (C.S) was equal to equation (1).

$$C.S = \frac{9 \lambda}{B \cos \theta} \quad (1)$$

where  $\lambda$  is the X-ray wavelength, B is the full width at half maximum (FWHM), and  $\theta$  is the diffraction angle. Using the TT diffractometer's software, the C.S was 12 nm with a FWHM of 0.0126, a radius  $2\theta = 25.57^\circ$ , and  $\lambda = 0.156\text{nm}$ .

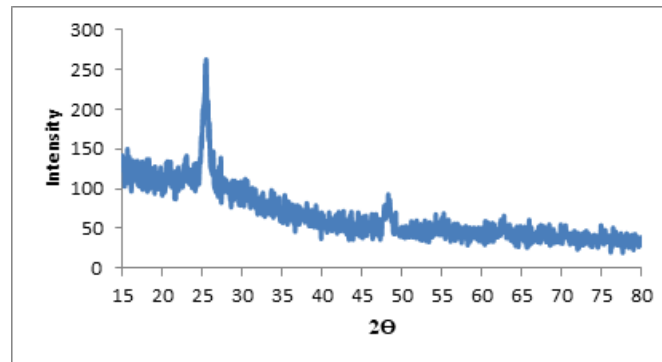


Fig 2. XRD patterns of the nc-TiO<sub>2</sub> film

Figure 3 shows SEM micrographs of the nc-TiO<sub>2</sub> film coated with a compact TiO<sub>2</sub>/SnO<sub>2</sub>:F<sub>n</sub> layer. The film surface consisted of agglomerates of nano sized particles (grains) distributed on the substrate surface. The SEM image revealed that the film's surface was rough because of these nano particles. That increased the interfacial area between the holes and electron transport layers by improving the dye penetration through the nano pores that formed at the particle interfaces. Figure 3 shows the cross-sectional area of the nc-TiO<sub>2</sub> film deposited using a scalpel. It is clear that the thickness of the nc-TiO<sub>2</sub> dominated the device's entire thickness. Its thickness was almost 1.7 μm, similar to values reported in the literature. The influence of the Ru dye encapsulation on the sample's surface can be seen clearly in the device's capacitance spectra.

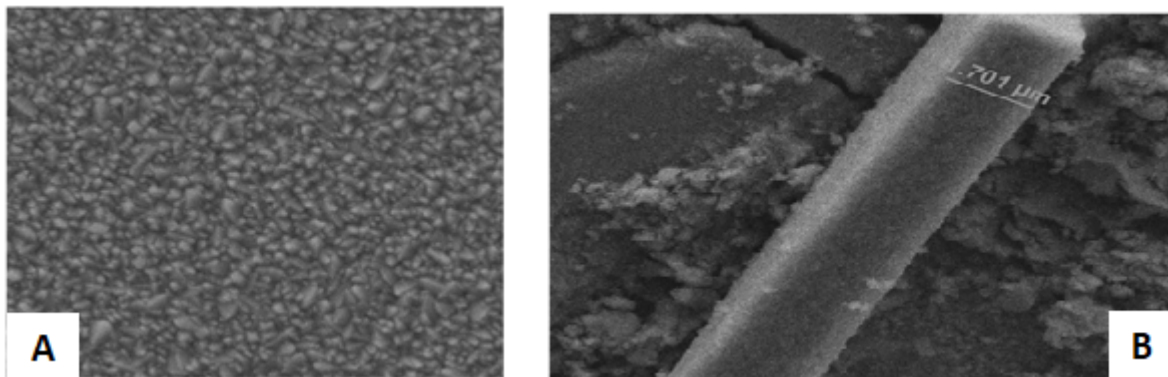


Fig 3. (a) Top view and (b) cross-sectional SEM images of the nc-TiO<sub>2</sub> film

Figure 4 presents the capacitance vs voltage measurements of the P3HT/Rudye/CB7/nc-TiO<sub>2</sub> solar cells at three different fixed frequencies. The devices were under reverse bias when the voltage was 1V to 0V and under forward bias from 0V to 1V. In three cases, the devices' capacitance was dominated by the dielectric constant of layers of solar cells under reverse bias. Therefore, the capacitance was independent of the applied voltage. The capacitance further increased at an applied voltage of -0.8V at frequencies of 10 KHz and 1KHz. In the latter case, the capacitance increased to a maximum before decreasing to zero at 1000Hz. It then decreased rapidly to become negative at 0 voltage bias at a frequency of 20Hz. That may have been due to the interfacial properties contribution to the total capacitance.

Figure 5 presents the variations in the ways the capacitance changed with the voltage applied on electrode of non-encapsulated device (P3HT/Rudye/nc-TiO<sub>2</sub> solar cells). The devices' different electron contacts. A sudden increase occurred and the maximum capacitance shifted to higher forward voltages as the frequency increased, although the capacitance decreased significantly

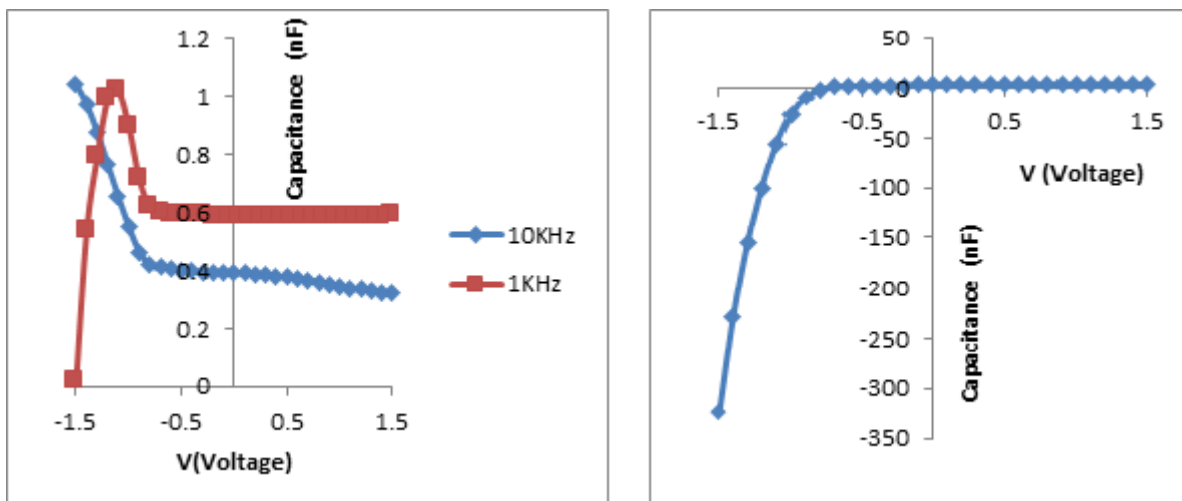


Fig 4. Capacitance vs voltage characteristics of the 3HT/Z907dye/CB7/nc-TiO<sub>2</sub> at 10kHz, 1KHz, and 20Hz

less. The capacitance was almost constant at an applied voltage of 10 KHz and started to increase slowly at -1.3V, higher by 0.4V than the encapsulated device. By decreasing the frequency to 1000Hz and 20 Hz, these solar cells demonstrated behaviour similar to the encapsulated device, although the negative capacitance value was smaller than one order of magnitude at -1.5V and 20Hz and did not decrease the capacitance at 1000Hz.

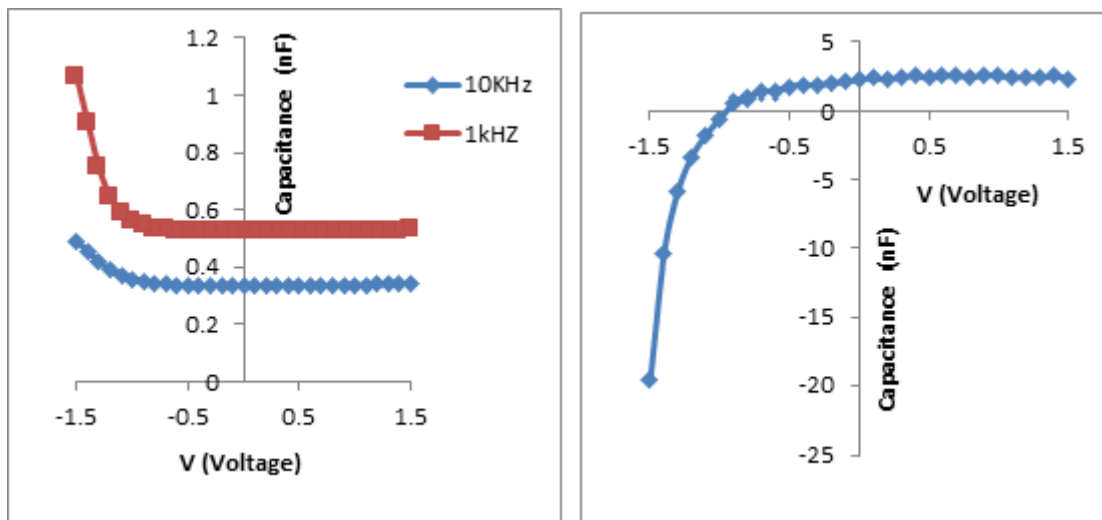


Fig 5. Capacitance vs voltage characteristics of the P3HT/Z907dye/nc-TiO<sub>2</sub> at 10kHz, 1KHz, and 20Hz

In the literature, the frequency dispersion during capacitance-voltage measurements of solar cells has been well documented<sup>(16)</sup>. Generally, if the AC voltage of the angular frequency  $\omega$  is applied across the solar cells, their bands will change as function of the voltage<sup>(17)</sup>. It depends on the charges flowing through the interfacial layers where the generation or recombination of charges occurs. From the results of the study and the literature, the solar cells' equivalent circuit may have fit the dispersion of combinations of resistors and capacitors shown in Figure 6.  $C_j$  and  $R_j$  represent the junction capacitance and resistance,  $C_g$  and  $R_g$  indicate the geometric resistance and capacitance, and  $R_s$  is the series resistance of the substrate and electrodes. The complex admittance (Cole-Cole plot) of the two devices at zero bias was also investigated.

Figure 7 shows two Cole-Cole curves revealing dispersion between 100Hz to 40Hz, which was more obvious in the non-encapsulated device corresponding to the region with almost constant loss. At low frequencies, additional dispersion occurred, increasing the devices' capacitance and loss. The two processes were caused by the components and interfacial layers since the

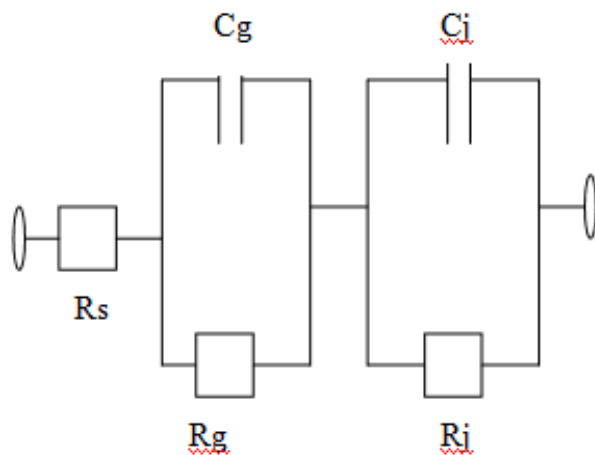


Fig 6. Simplified DC equivalent circuit of the P3HT/Z907 dye/CB7/nc-TiO<sub>2</sub> solar cells

whole conductor in the solar cells was a p-type organic semiconductor, P3HT, and nc-TiO<sub>2</sub> electron transport material<sup>(17,18)</sup>. Similar to Theivasanthi’s study<sup>(14)</sup>, flat capacitive responses occurred with respect to high frequency and under reverse bias condition. It was dominated by the geometrical structure of the capacitor ( $C_{geo}$ ). At a high frequency, the capacitance was constant, which was attributed to the thermal generation and recombination of charge carriers and did not follow the AC modulation.

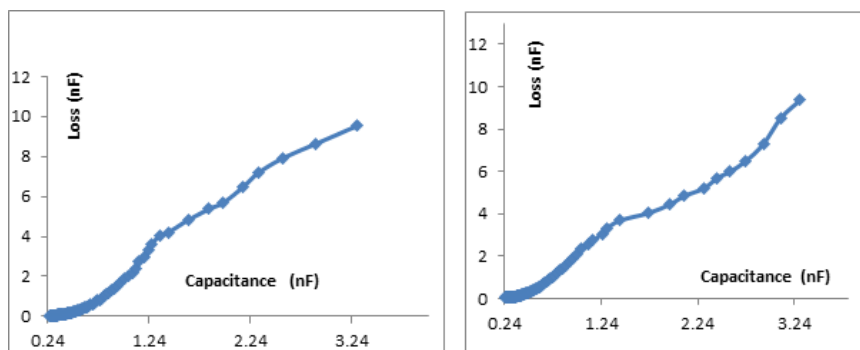


Fig 7. Cole-Cole plot of the(a) P3HT/Z907 dye/CB7/nc-TiO<sub>2</sub> and (b) P3HT/Z907/nc-TiO<sub>2</sub> solar cells

According to previous studies<sup>(3,18,19)</sup>, the interfacial region’s properties cannot be investigated at reverse bias and high frequencies. The data demonstrated that the capacitance increased with the voltage, and the dispersion of the Cole-Cole plot appeared at low frequencies. This behaviours may be explained using the equivalent circuit in Figure 8. Solar cells have two main regions: junction and bulk regions. At frequencies below 7.5 kHz, the high resistivity of the nc-TiO<sub>2</sub> and P3HT phase shunt its bulk region capacitance and dominate the junction capacitance and whole measurements. The appearance of junction capacitance depends on defect states within the band gap and the accumulation of charge density near the interfaces<sup>(18)</sup>. In this study, the encapsulated device demonstrated higher capacitance response to forward bias than the non-encapsulated device at the same frequency. That was evidence of the encapsulating dye on the nc-TiO<sub>2</sub> suppressing the dye aggregation on its surface which is undesirable in these types solar cells and can affect the concentration of accumulation charge at the interfaces and the way of following states the ac signal. To investigate the transfer charge dynamic through the interfacial layers, the devices’ capacitance was measured as a function of the frequency at different voltage biases. Figures 8 and 9 show the capacitance frequency plots of the two devices. The voltage was applied on the SnO<sub>2</sub>: Fn electrodes. The forward bias condition started from 0V to -1V as the reverse bias condition increased from 0V to 1V. In the two devices, the series resistance and bulk region capacitance of the components dominated the high-frequency capacitance. The measured capacitance decreased because the frequency was lower than the charge carriers’ relaxation time. In this case, the junction capacitance contributed to the overall

capacitance. The decrease was ascribed to charge carriers that lagged behind the AC field variations at the junction. That was because the junction capacitance was controlled by the region of depleted capacitance and the decrease in the charge carriers that accumulated at the junction at frequencies ranging from 100Hz to 20 Hz at -0.8V. However, at -1.5V, the low-frequency capacitance was dominated by the diffusion capacitance because of the absence of the depletion region. This was caused by the accumulation of charge carriers at the interfaces. The results demonstrate the high negative capacitance in encapsulated device because 1) the encapsulating dye enabled the injection of accumulated charge carriers and 2) dipoles were present at the junctions<sup>(20,21)</sup>. This decreased the capacitance in the negative region and increased the loss in the solar cells without encapsulating dye by more than three times.

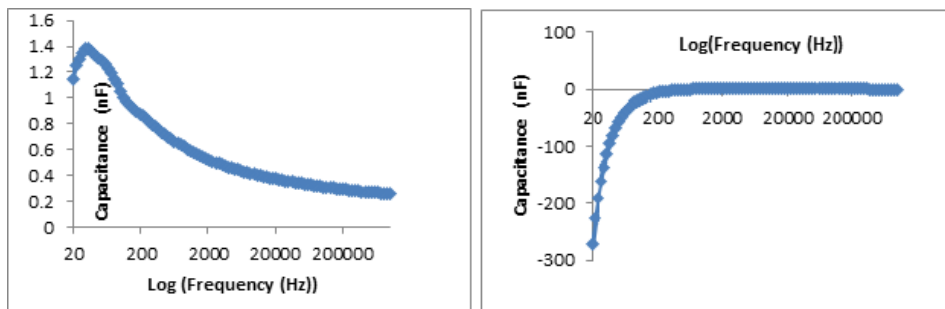


Fig 8. Capacitance-frequency characteristics of the P3HT/Z907dye/CB7/nc-TiO<sub>2</sub> solar cells at -0.8V and -1.5V

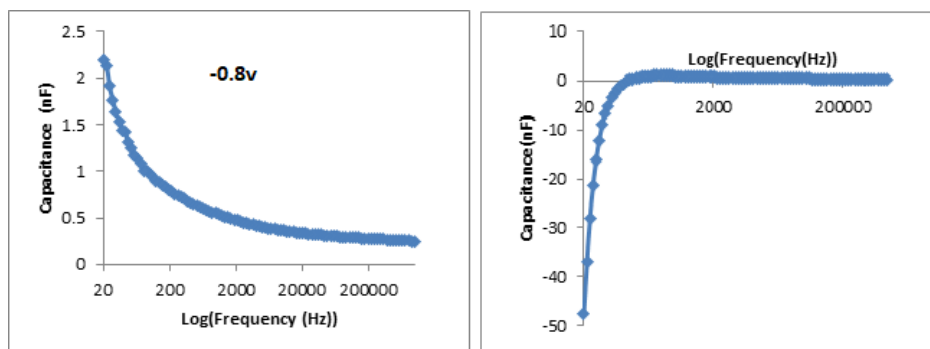


Fig 9. Capacitance-frequency characteristics of the P3HT/Z907dye/nc-TiO<sub>2</sub> solar cells at -0.8V and -1.5V

The devices' power characteristics are presented in Figure 9. The encapsulated device's maximum electric power increased from 0.04mW/cm<sup>2</sup> to 0.14mW/cm<sup>2</sup>, 150% improvement. These results confirmed that the CB7and dyes'host-guest complexes increased the exciton (hole electrons) injection of the Z907 dye into the of TiO<sub>2</sub>

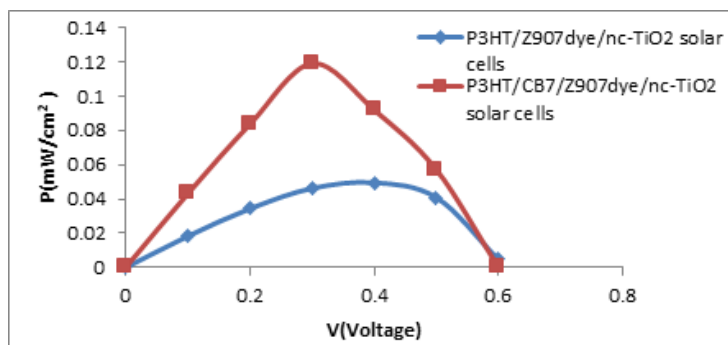


Fig 10. Electric power vs voltage applied to the P3HT/CB7/Z907dye/TiO<sub>2</sub> solar and P3HT/Z907dye/TiO<sub>2</sub> solar cells

## 4 Conclusion

Encapsulation of the Z907 dye-sensitized TiO<sub>2</sub> surface changed the interfacial layers of the P3HT/Z907 dye/TiO<sub>2</sub> solar cells, causing a higher capacitance response to forward bias and higher negative capacitance than in the non-encapsulated device at the same frequency. That was considered evidence that the encapsulating dye on the nc-TiO<sub>2</sub> suppressed the dye aggregation on its surface. It also generated higher electric power in the encapsulated solar cells than on the unmodified TiO<sub>2</sub> surface.

## References

- 1) Ammar AM, Mohamed HSH, Yousef MMK, Abdel-Hafez GM, Hassanien AS, Khalil ASG. Dye-Sensitized Solar Cells (DSSCs) Based on Extracted Natural Dyes. *Journal of Nanomaterials*. 2019;2019:1–10. doi:10.1155/2019/1867271.
- 2) Liao Y, Lin P, Chen Y, Kuang B, Su Y. High-performance dye-sensitized solar cells based on hierarchical yolk-shell anatase TiO<sub>2</sub> beads. *Journal of Materials and Chemistry*. 2012;22(4):1627–1633. doi:10.1039/c1jm14489h.
- 3) Al-Dmour H, Taylor DM, Cambridge JA. Effect of nanocrystalline-TiO<sub>2</sub> morphology on the performance of polymer heterojunction solar cells. *Journal of Physics D: Applied Physics*. 2007;40(17):5034–5038. doi:10.1088/0022-3727/40/17/004.
- 4) Fitra M, Daut I, Irwanto M, Gomes N, Irwan YM. Effect of TiO<sub>2</sub> Thickness Dye Solar Cell on Charge Generation. *Energy Procedia*. 2013;36:278–286. doi:10.1016/j.egypro.2013.07.032.
- 5) Yan M, Lane M, Kannewurf CR, Chang RPH. Highly conductive epitaxial CdO thin films prepared by pulsed laser deposition. *Applied Physics Letters*. 2001;78(16):2342–2344. doi:10.1063/1.1365410.
- 6) Fortunato E, Barquinha P, Martins R. Oxide Semiconductor Thin-Film Transistors: A Review of Recent Advances. *Advanced Materials*. 2012;24(22):2945–2986. doi:10.1002/adma.201103228.
- 7) Zhang L, Cole JM. Dye aggregation in dye-sensitized solar cells. *Journal of Materials Chemistry A*. 2017;5(37):19541–19559. doi:10.1039/c7ta05632j.
- 8) Wang ZS, Cui Y, Dan-oh Y, Kasada C, Shinpo A, Hara K. Thiophene-Functionalized Coumarin Dye for Efficient Dye-Sensitized Solar Cells: Electron Lifetime Improved by Coadsorption of Deoxycholic Acid. *The Journal of Physical Chemistry C*. 2007;111(19):7224–7230. doi:10.1021/jp067872t.
- 9) Ito S, Zakeeruddin SM, Humphry-Baker R, Liska P, Charvet R, Comte P, et al. High-Efficiency Organic-Dye-Sensitized Solar Cells Controlled by Nanocrystalline-TiO<sub>2</sub> Electrode Thickness. *Advanced Materials*. 2006;18(9):1202–1205. doi:10.1002/adma.200502540.
- 10) Schölin R, Quintana M, Johansson EMJ, Hahlin M, Marinado T, Hagfeldt A, et al. Preventing Dye Aggregation on ZnO by Adding Water in the Dye-Sensitization Process. *The Journal of Physical Chemistry C*. 2011;115(39):19274–19279. doi:10.1021/jp206052t.
- 11) Choi H, Kang S, Ko J, Gao G, Kang H, Kang MS, et al. An Efficient Dye-Sensitized Solar Cell with an Organic Sensitizer Encapsulated in a Cyclodextrin Cavity. *Angewandte Chemie International Edition*. 2009;48(32):5938–5941. doi:10.1002/anie.200902013.
- 12) Al-Dmour H, Taylor DM. Small-signal response of nanocrystalline-titanium dioxide/poly(3-hexylthiophene) heterojunction solar cells. *Thin Solid Films*. 2011;519(22):8135–8138. doi:10.1016/j.tsf.2011.06.009.
- 13) Al-Dmour H, Alzard RH, Alblooshi H, Alhosani K, AlMadhoob S, Saleh N. Enhanced Energy Conversion of Z907-Based Solar Cells by Cucurbit[7]uril Macrocycles. *Frontiers in Chemistry*. 2019;7(561):1–9. doi:10.3389/fchem.2019.00561.
- 14) Theivasanthi T, Alagar M. Titanium dioxide (TiO<sub>2</sub>) Nanoparticles - XRD Analyses – An Insight. 2013. Available from: <https://arxiv.org/abs/1307.1091>.
- 15) C K. Introduction To Solid State physics. Wiley publisher edition. 2004.
- 16) Wang Y, Tseng Y. Analysis of AC electrical response for radio-frequency sputtered (Ba<sub>0.5</sub>Sr<sub>0.5</sub>)TiO<sub>3</sub> thin film. *Thin Solid Films*. 1999;346(1-2):269–274.
- 17) Kulkarni AP, Tonzola CJ, Babel A, Jenekhe SA. Electron Transport Materials for Organic Light-Emitting Diodes. *Chemistry of Materials*. 2004;16(23):4556–4573. doi:10.1021/cm049473l.
- 18) Juarez-Perez E. Photoinduced Giant Dielectric Constant in Lead Halide Perovskite Solar Cells. *The Journal of Physical Chemistry Letters*. 2014;5(13):2390–2394. doi:10.1021/jz5011169.
- 19) Wang C, Li J, Cai S, Ning Z, Zhao, Zhang Q, et al. 2012.
- 20) Westermarck, Henningsson A, Rensmo H, Soedergrén S, Siegbah H, Hagfeldt. Electronic Density of States at a Nanostructured TiO<sub>2</sub>/Ru-dye/Electrolyte Interface by Means of Photoelectron Spectroscopy. *Chemical Physics*. 2002;285(1):157–165. doi:10.1016/s0301-0104(02)00699.
- 21) Ravishankar S, Gharibzadeh S, Roldán-Carmona C, Grancini G, Lee Y, Ralaiarisoa M, et al. Influence of Charge Transport Layers on Open-Circuit Voltage and Hysteresis in Perovskite Solar Cells. *Joule*. 2018;2(4):788–798. doi:10.1016/j.joule.2018.02.013.